Agricultural and Forest Meteorology 353 (2024) 110042

Contents lists available at ScienceDirect

Agricultural and Forest Meteorology

journal homepage: www.elsevier.com/locate/agrformet

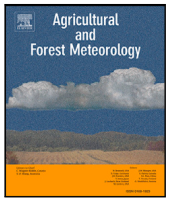

Evaluating the nature of turbulent coherent structures in orchards using integrated quadrant analysis

Mary Rose Mangan [a,b,*], Holly J. Oldroyd [c], Kyaw Tha Paw U [a], Jenae M. Clay [a], Kosana Suvočarev [a]

[a] Department of Land, Air and Water Resources, University of California, Davis, CA, USA
[b] Meteorology and Air Quality, Wageningen University and Research, Wageningen, The Netherlands
[c] Department of Civil and Environmental Engineering, University of California, Davis, CA, USA

ARTICLE INFO

Keywords:
Canopy turbulence
Integrated quadrant analysis
Coherent structures
VACE
CHATS

ABSTRACT

Inside orchards, turbulent coherent structures dominate the transport of heat, momentum, and moisture between the canopy and the atmosphere. Integrated quadrant analysis is a method to visualize the trajectory of individual turbulent coherent structures using in situ data from three-dimensional anemometry. In this paper, integrated quadrant analysis is used to characterize the turbulent transport of heat and momentum from two orchard experiments: one in the interrow space (the Canopy Horizontal Array Turbulence Study from Dixon, California in May and June 2007) and one in the crown of a tree (the Vertical Array Cherry Experiment from Linden, California in November 2019). By using the integrated quadrant analysis (IQA) method, this paper demonstrates the importance of the cross-wind velocity component in maintaining the turbulent coherent structures. Results from integrated quadrant analysis in three dimensions support the idea that the microfront is collocated with the boundary of a sweep and an ejection in a convective boundary layer. Moreover, in both orchards, there are preferred planar trajectories for individual coherent structures that do not depend on wind regimes. The statistical profile of the turbulence quantities, as well as individual coherent structures, are not appreciably different in the interrow space or within the crown.

1. Introduction

Plant canopy turbulence is an important mechanism for transporting momentum, heat, and trace gases between the surface, vegetation, and the atmosphere. Unlike turbulence above idealized flat, homogeneous surfaces, the canopy contains spatially distributed sources and sinks of heat and momentum, which add complexity to understanding surface–atmosphere interactions. Heat, momentum, and greenhouse gas fluxes between canopies and the atmospheric surface layer are mostly driven by large-scale, organized turbulence called turbulent coherent structures (Finnigan, 1979, 2000; Paw U et al., 1992; Raupach, 1981; Raupach et al., 1996). Various analytical methods have been used to dissect the details of turbulent coherent structures using experimental field data and Large Eddy Simulation output. These include various forms of conditional sampling, including variable-interval time-averaging, two point statistics, wavelets, and Empirical Orthogonal Function (Blackwelder and Kaplan, 1976; Bisset et al., 1990; Chen and Blackwelder, 1978; Farge, 1992; Collineau and Brunet, 1993; Finnigan, 2000; Thomas and Foken, 2005; Wallace et al., 1972).

Raupach et al. (1996) proposed the mixing layer analogy to explain the formation of turbulence in vegetation. Near the top of the canopy, air flow resembles that of a mixing layer plane between the slower moving air in the canopy and the faster moving air above the canopy. This is evident in the inflection point at the top of the canopy in velocity profiles. At the boundary between these two flow regimes near the top of the canopy, the strong wind shear creates a Kelvin–Helmholtz-like instability, which breaks down into hairpin (also called horseshoe) vortices (Theodorsen, 1952 as cited by Adrian (2007)) that infiltrate through the vegetation. In an idealized case, the hairpin vortices occur in pairs consisting of a head-down hairpin vortex – a sweep – and a head-up hairpin vortex — an ejection (Finnigan, 2000; Finnigan et al., 2009). Alternative interpretations of the shape of shear-driven coherent structures have been postulated. For example, Bernard (2011) suggested that coherent structures are "mushroom-like" packets of vorticity structures.

Using quadrant analysis (Wallace et al., 1972), Raupach (1981) shows that over a rough surface, sweeps account for a larger portion

* Corresponding author at: Meteorology and Air Quality, Wageningen University and Research, Wageningen, The Netherlands.
E-mail address: maryrose.mangan@wur.nl (M.R. Mangan).

https://doi.org/10.1016/j.agrformet.2024.110042
Received 14 July 2023; Received in revised form 28 February 2024; Accepted 30 April 2024
Available online 22 May 2024

of shear stress than ejections. Dupont and Patton (2012) used quadrant analysis to find that under near-neutral conditions, momentum transport occurred primarily through sweeps using data from National Center for Atmospheric Research's (NCAR) Canopy Horizontal Array Turbulence Study (CHATS). Under no-leaf conditions, sweeps dominate at the height above the ground (Z) normalized by the canopy height (h) (Z/h) of 0.4 and ejections begin to dominate above the canopy at $Z/h = 1.4$. When the canopy is foliated, however, the sweeps are not able to penetrate as deeply into the canopy.

In addition to quadrant analysis, scalar signals can be used to trace coherent structures. For example, coherent structures have been observed with the temperature signal in laboratory experiments (Chen and Blackwelder, 1978) and atmospheric experiments (Priestley, 1959; Wilczak, 1984; Gao et al., 1989; Shaw et al., 1989). Under unstable conditions, a gradual temperature rise is followed by an abrupt temperature decrease called a microfront. Gao et al. (1989) saw that during stable conditions, the temperature ramps are reversed so that a gradual temperature decrease is followed by a sharp temperature increase at the microfront. Although temperature ramps were originally believed to be due to thermals, they have also been observed under near-neutral conditions (Antonia and Atta, 1978). This indicates that temperature ramps can be shear-driven (Paw U et al., 1992). Under unstable (stable) conditions, the temperature drop (rise) represents an ejection followed by a sweep in a coherent structure. Gao et al. (1989) showed that the microfront is lagged in time as the sweep penetrates the canopy.

In addition to measurement campaigns, numerical models have been used to show the structure of canopy turbulence. Multiple Large-Eddy Simulation (LES) studies have found that in canopies, a relatively weak ejection tends to be followed by a strong sweep (Fitzmaurice et al., 2004; Watanabe, 2004; Finnigan et al., 2009). Physically, this relates to the mixing layer theory of turbulent generation proposed by Raupach et al. (1996). Moreover, LES results indicate that the cross-stream velocity field diverges in order to balance the convergence of the streamwise and vertical velocity fields (Fitzmaurice et al., 2004). This mechanism is important for maintaining coherent structures' integrity as they traverse within and above canopies.

Many measurement campaigns have focused on flow inside canopies, including forests (Baldocchi and Meyers, 1988; Denmead and Bradley, 1987; Hari et al., 2013; Shaw et al., 1989; Gao et al., 1992) and cropland Shaw et al. (1974) and Wilson et al. (1982), measuring the turbulence in open spaces between rows or in clearings. However, when the measurements are applied to turbulent flow, conditions should be horizontally averaged to represent the entire flow volume. Wilson and Shaw (1977) and Raupach and Shaw (1982) show that spatial averaging in a canopy includes the flow between and within the open spaces and the vegetation. The horizontal averaging schemes are important for any of the three-dimensional canopy flow equations and must account for components such as canopy drag. Typically, the wake-production terms, which are not often measured, are assumed to be negligible in horizontal averaging schemes (Wilson and Shaw, 1977). There are few measurement campaigns where instruments were located adjacent to or within the crown of a tree. The Vertical Array Cherry Experiment (VACE) contains a vertical array of sonic anemometers that are located adjacent to a crown of a cherry tree (Mangan et al., 2022).

Properties of orchard turbulence will be evaluated with data from two orchard campaigns: VACE (sensors adjacent to the crown) and CHATS (sensors between the rows). Each dataset contains periods with and without leaves, as different canopy drag may significantly affect canopy turbulence (Shaw et al., 1989). This study aims to compare the turbulence adjacent to a crown with the turbulence in the inter-row space of orchards by comparing VACE and CHATS observations, respectively. By using Integrated Quadrant Analysis (IQA) (Mangan et al., 2022) to visualize the motion of the coherent structures in three-dimensions, the Eulerian measurements can be connected to the idealized model of hairpin vortices. Furthermore, the role of the cross-stream velocity component and the tilt of eddies through the canopy will be evaluated to investigate the structure of turbulence in two case studies. We choose to analyze case studies both because IQA is a relatively new method that needs to be more thoroughly tested, and case studies allow us to focus on the details of the mechanisms of turbulent transport.

2. Materials and methods

2.1. Experimental data

In this section, we will describe both canopy turbulence experiments examined in this study: VACE (Section 2.1.1) and CHATS (Section 2.2). In Section (Section 2.2), we introduce the method of IQA. Because IQA is a new method to characterize turbulent coherent structures, this analysis demonstrates the benefits of using IQA compared to other methods for evaluating turbulence. One case study for each experiment was selected to show here.

2.1.1. Vertical array cherry experiment

The Vertical Array Cherry Experiment (VACE) was active from November 2019 through July 2020 in Linden, California in the northern San Joaquin Valley. This experiment was conducted for the purpose of testing IQA inside of a canopy. The cherry (*Prunus avium*) orchard had a north–south row orientation with a tree spacing of 6 m between the trees within the rows. The interrow had a width of approximately 7 m. This orchard was microsprinkler-irrigated approximately once per week during the spring time. The canopy top was maintained at 3.6 m by mechanical pruning. There was some change in tree height due to new growth between prunings. In November 2019, the height of the canopy was 3.6 m tall, and by April 2020, the canopy height was approximately 4 m. VACE was split up into three distinct measurement periods: a fall measurement period in November 2019, a winter measurement period in January 2020, and a spring measurement period in March and April 2020. We refer to Fig. 1 in Mangan et al. (2022) for a graphical description of the experimental design of the VACE experiment.

The November measurement period was characterized by leaves on the trees and no irrigation. The November period will hereafter be referred to as the "leaf" period of VACE. This experiment period lasted from November 8 through November 25, 2019. During this period, there were five ultrasonic anemometers (CSAT3, Campbell Scientific Inc., Logan, Utah, USA) oriented on the northwest corner of scaffolding structure pointed into the predominant wind at the heights of 1.5 m, 2.2 m, 3.0 m, 3.9 m and 5.8 m. The anemometers were sampled at 20 Hz and were logged in the same data logger synchronous device for measurement (SDM) protocol to ensure continuity in the timestamps in all five sensors. All sonic anemometers were pointing to the northwest at 310° from north. There were two fine wire thermocouples located at 3.9 m and 5.8 m that were sampling at 20 Hz. In addition to fast response instruments, an NR-Lite net radiometer (Kipp & Zonen) and ground heat flux plates were co-located at the site for measuring the surface energy budget.

The winter measurement period lasted from 10 January through 22 January 2020. During this period, there were no leaves on the trees, but there was grass in the interrow. This period will be referred to as the "leafless" period. The experimental design was the same as the previous period, except the anemometer located at 1.5 m was removed. The spring measurement period lasted from 29 March through 16 April 2020. During this period there were green, transpiring leaves on the trees. This period will be referred to as the "leaf-out" period. The ultrasonic anemometers and fine-wire thermocouples were in the same locations during the leafless measurement period.

Velocity components were rotated into the mean wind for all analyses at each height. The data were not tilt corrected because the measurement location was heterogeneous. Instead, the anemometers were carefully leveled with a bubble level. Moreover, there were likely true vertical velocity components in this study — mean pitch angles

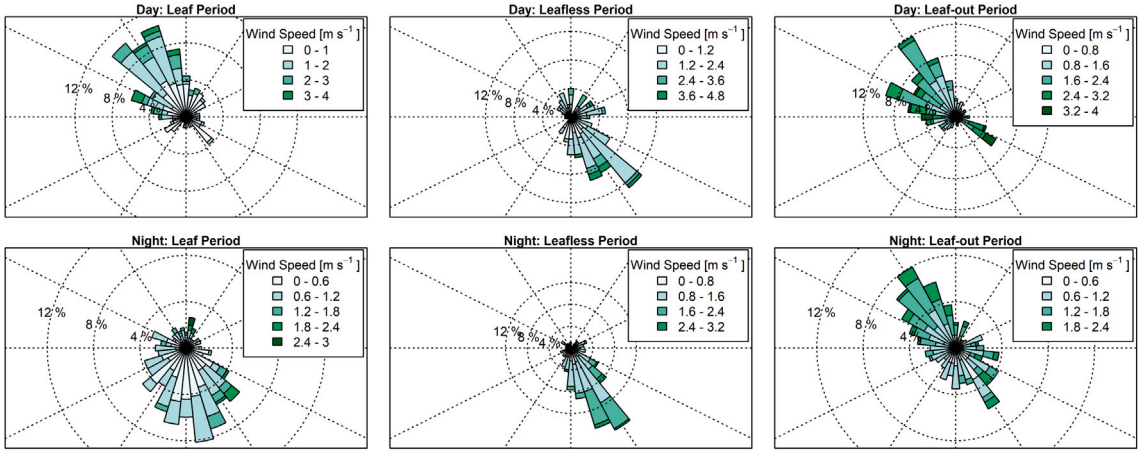

Fig. 1. Wind Roses for the anemometer located at 5.8 m (Z/h = 1.6) for VACE. Daytime hours were between 07:00–17:00 PST, and nighttime is 17:00–07:00 PST.

were as high as 80° under very stable conditions with low wind speeds. Therefore, a single rotation scheme would have less errors than the double rotation scheme when vertical velocities are present.

During the leaf and leaf-out measurement periods, the predominant wind direction was from the northwest during the day (Fig. 1). At night, the wind direction tended to shift to the southeast. In the leafless period, the predominant wind was from the southeast for both daytime and nighttime. When wind directions are from the southeast, the crown of the tree could block the wind before it reaches the anemometers. In the leaf-out period, the predominant wind returns to the northwest. In the leafless and leaf-out measurement periods, the mean wind speed is 1.2 m s^{-1} at 5.8 m . In leaf period, the mean wind speed is 0.8 m s^{-1} at 5.8 m.

During the day, the wind regime is controlled by regional-scale flow. The measurement location is in the Central Valley of California, and surface winds are controlled by the "delta breeze" from the Sacramento-San Joaquin Delta (Zaremba and Carroll, 1999). During the day, cool and wet air is advected inland from the Sacramento-San Joaquin Delta, which is to the northwest of this site. Overnight, a land breeze dominates, so the wind direction changes to southeasterly. In the winter period of VACE, when the temperature contrast is minimum between the land and sea, the delta breeze effect is minimal. Instead, wintertime and early springtime winds are controlled by the synoptic scale weather patterns.

Wind directional shear has been shown to occur in canopies with both observations and numerical simulations (Misson et al., 2007; Pyles et al., 2004; Smith et al., 1972). The directional shear in the canopies is loosely analogous to the Ekman spiral. Near the no-slip condition at the surface, where friction and pressure gradient forces dominate, the flow can be close to antitriptic, meaning that the flow is tends towards being perpendicular to isobars, from high to low pressure. Within the canopy, drag elements, like branches and leaves, and above the canopy, are associated with turbulent transfer transporting momentum stress (as a vector), eventually turning the wind direction into the geostrophic wind parallel to isobars, above the planetary boundary layer. The leaf area index and canopy structure and distribution impact the extent of the directional wind shear (Pyles et al., 2004) found that the high leaf area indexes, especially when the LAI is concentrated in the canopy, have greater directional shear than less dense canopies. The directional shear observed in VACE for the November period is consistent with these simulations, observations, and theory.

2.1.2. Canopy horizontal array turbulence study

The CHATS experiment studied turbulence in a 10 m tall walnut orchard in Dixon, California from March through June 2007 (Patton et al., 2011). CHATS included extensive turbulence measurements including a horizontal array consisting of five 12 m towers arranged in a transect and a single 30 m tower. The data were split into two periods: before and after leaf-out. Although CHATS also includes a horizontal array of anemometers, only anemometer data from the 30 m tall tower are used in this study.

The 30 m tower had 13 ultrasonic anemometers (CSAT3, Campbell Scientific Inc., Logan, Utah, USA) placed between 1.5 m and 29 m above ground level. All anemometers faced west. Five anemometers were in the canopy, one was at the canopy top and seven were located between 1 and 20 m above the canopy. The anemometers sampled at 60 Hz, but for this analysis, the data were downsampled to 20 Hz. The maximum fetch was in the south and southwest directions. Several periods of predominantly southern winds were chosen for the study to ensure data quality: one before leaf-out and two after leaf-out (Fig. 2).

CHATS data are available for public download in 5-minute averages and raw data at 60 Hz (Horst, 2019). For the raw data, there were three periods used in the analysis: 1–10 April, 18–19 May, and 4–9 June 2007. The raw data were tilt corrected with a planar fit rotation (Paw U et al., 2000; Wilczak et al., 2001) that was calculated for each height for each of the before and after leaf-out periods. The velocity field also was rotated into the mean wind for each height in the analysis. Fig. 2 shows that the predominant wind direction during the night was from the south. During the day, in the April (leafless) period, about half of the time periods had northerly winds and half had southerly winds. The northerly winds were generally faster than the southerly winds. The June (leaf) period had winds predominantly from the south.

2.2. Integrated quadrant analysis

IQA is a conditional sampling method to identify and to visualize the trajectories of turbulent coherent structures (Mangan et al., 2022). Unlike statistical methods for detecting turbulent coherent structures like wavelet analysis and quadrant analysis, IQA aims to analyze the phenomena of turbulent transport at the scale of individual eddies. Furthermore, it connects ejections and their subsequent sweeps together in time and in space, which allows one to focus on the physics of turbulent transport in the surface layer.

There are two steps required to employ IQA: (1) detect individual coherent structures, and (2) compute IQA in three dimensions. Because IQA is computed as an integration of the 3D velocity field in time, its values depend on an arbitrary starting point. Therefore, a method was needed to determine the start of an individual coherent structure.

Although there are many methods to identify the presence of a structure – including visual identification of temperature ramps (Paw U et al., 1992), variable-interval time-averaging (Blackwelder and Kaplan, 1976), and wavelet transforms (Farge, 1992) – existing methods locate the start of a structure at the microfront. A coherent structure identification method was paired with IQA to identify the start of the

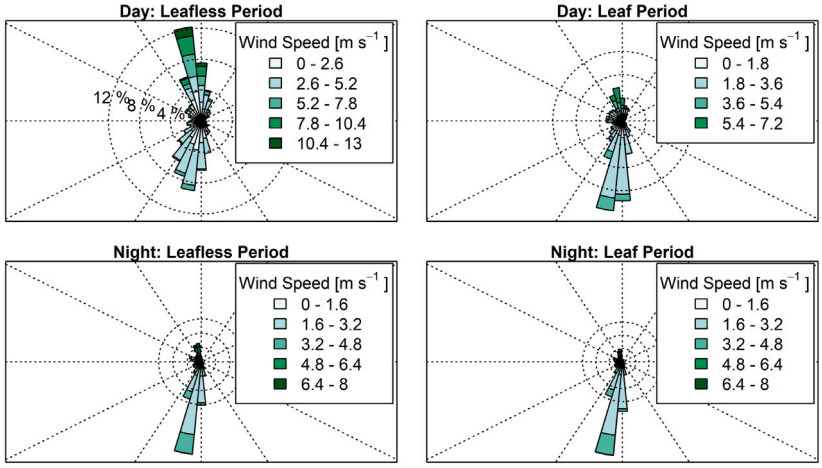

Fig. 2. The wind roses for the leafless and leaf period for CHATS from 5 min wind data. The night plots are between 20:00–7:00 PST. The day plots are between 7:00–20:00 PST at $Z/h = 1.4$.

structure in the ejection phase so that one event consists of the ejection, the subsequent sweep, and the quiescent period between coherent structures. The coherent structure identification method used in this study is based on the high-frequency signal of a velocity scale based on the turbulent kinetic energy ($uTKE = \sqrt{\overline{u'^2} + \overline{v'^2} + \overline{w'^2}}$). To summarize the identification procedure, coherent structures are identified using the Mexican hat wavelet transformation on the low pass filtered $uTKE$ signal. In this method, individual coherent structures are identified at the start of sweep phase and encompass the subsequent ejection and quiescent period before the next coherent structure. We refer to Fig. 3 in Mangan et al. (2022) for more details about the coherent structure identification method and a discussion of why $uTKE$ was determined to be the best structure identification parameter.

To compute IQA, the streamwise (u), crosswind (v) and vertical velocities (w) are first Reynolds-averaged over a half-hour averaging period to calculate the deviations from the mean. Each fluctuating component is integrated with respect to time to calculate integrated distance along each axis. The recursive integration is described by Eqs. (1), (2) & (3) where X_i is the position for the streamwise component; Y_i is the position for the cross-stream component; Z_i is the position for the vertical velocity component, the subscript i indicates a time step(a data record point), and δt is the time interval between records in the data.

$$X_i = X_{i-1} + \left(u_i'\right)\delta t \tag{1}$$

$$Y_i = Y_{i-1} + \left(v_i'\right)\delta t \tag{2}$$

$$Z_i = Z_{i-1} + \left(w_i'\right)\delta t \tag{3}$$

X_i, Y_i and Z_i can be plotted or animated in two- or three-dimensions to visualize air flow trajectories of individual coherent structures. This method splits coherent structures into two regimes: bulk sweep ($Z_i > 0$) and bulk ejection ($Z_i < 0$). Additionally, distances in all directions can be summed over the structure or a period of time as a measure of size or strength of the individual coherent structure. Eq. (4) describes the summation over the integrated path for the X_i direction. This distance measure (X) is analogous to a three-dimensional wind run summed at every time step (i) through the duration of the turbulent coherent structure (n).

$$X_i = \sum_{i=1}^{n} \left| \left(u_i'\right)\delta t \right| \tag{4}$$

3. Results & discussion

In this study, we primarily focus on one case study from each the VACE and CHATS experiments in Section 3.1. We chose to focus on individual coherent structures to demonstrate the utility in using IQA to examine the dynamics of individual coherent structures. In addition to the case studies, in Section 3.2, we evaluate IQA statistics for each experiment to investigate the diurnal and seasonal cycle of coherent structures in orchards.

The case studies for both the VACE and CHATS experiments were selected based on stability and friction velocity to ensure that we could observe shear-based turbulence. Furthermore, we also filtered based on wind direction to ensure that the flow was coming from the orchards. Quality control of the data was embedded in our case study selection. Conversely, when we evaluate statistics of the turbulent coherent structures, we include periods with stable stratification and low turbulence so that we can evaluate the method under these conditions.

3.1. Integrated quadrant analysis: Case studies

IQA was calculated for one select time period from each of the VACE and CHATS experiments (Table 1). For this study, daytime periods from each site were selected based on wind direction (southerly or westerly winds for CHATS), high mean temperature ramp amplitudes (near 1°C), and $uTKE$ (greater than 0.3 m s^{-1}). For these case studies, the coherent structures were selected if IQA identified an event at all measurement levels at approximately the same time.

3.1.1. Vertical Array Cherry Experiment

On 16 November 2019, the selected VACE coherent structure was identified starting at 11:09 LT (UTC-8) using the levels $Z/h = 1.6$, 1.1, 0.8, 0.6 and 0.4. The coherent structure was identified 15 s earlier at $Z/h = 1.6$ than at $Z/h = 0.4$. This time lag is assumed to be the time it takes for the coherent structure to penetrate the canopy. Within the canopy, at $Z/h = 0.8$ and $Z/h = 0.6$, the event begins at approximately the same time. Above the canopy, the structure lasts about 160 s, but within the canopy, it lasts about 60 s. Fig. 3 shows the trace of the two-dimensional IQA trajectory colored by time. Please note that the X_i and Y_i axes' limits change for each height: at $Z/h = 1.6$, the X_i magnitude is almost 2.5 times the magnitude of the X_i scale at $Z/h = 0.4$.

At $Z/h = 1.6$ and $Z/h = 0.8$, the event begins with a weak bulk ejection before entering a bulk sweep. At the other heights, there is no discernible bulk ejection. The sweep lasts approximately 40 s at all levels except closest to the surface. At $Z/h = 0.4$, the structure begins with weak counter-gradient flux. The sweep starts 20 s after the start of the structure and lasts approximately 15 s. In the levels higher than $Z/h = 0.4$, the sweep is moving from the top left to the bottom right in the plot, however, at the lowest level, the sweep is showing little

Table 1
Selected case study times for VACE and CHATS.

Experiment	Date	Time	Wind Speed (Z/h~1.5) [m s^{-1}]	Wind Direction (Z/h~1.5) [°]	$uTKE$ (Z/h~1.5) [m s^{-1}]
VACE (Leaf)	16 November 2019	11:00	0.65	57	0.70
CHATS (Leaf)	6 June 2007	15:30	1.49	261	1.18

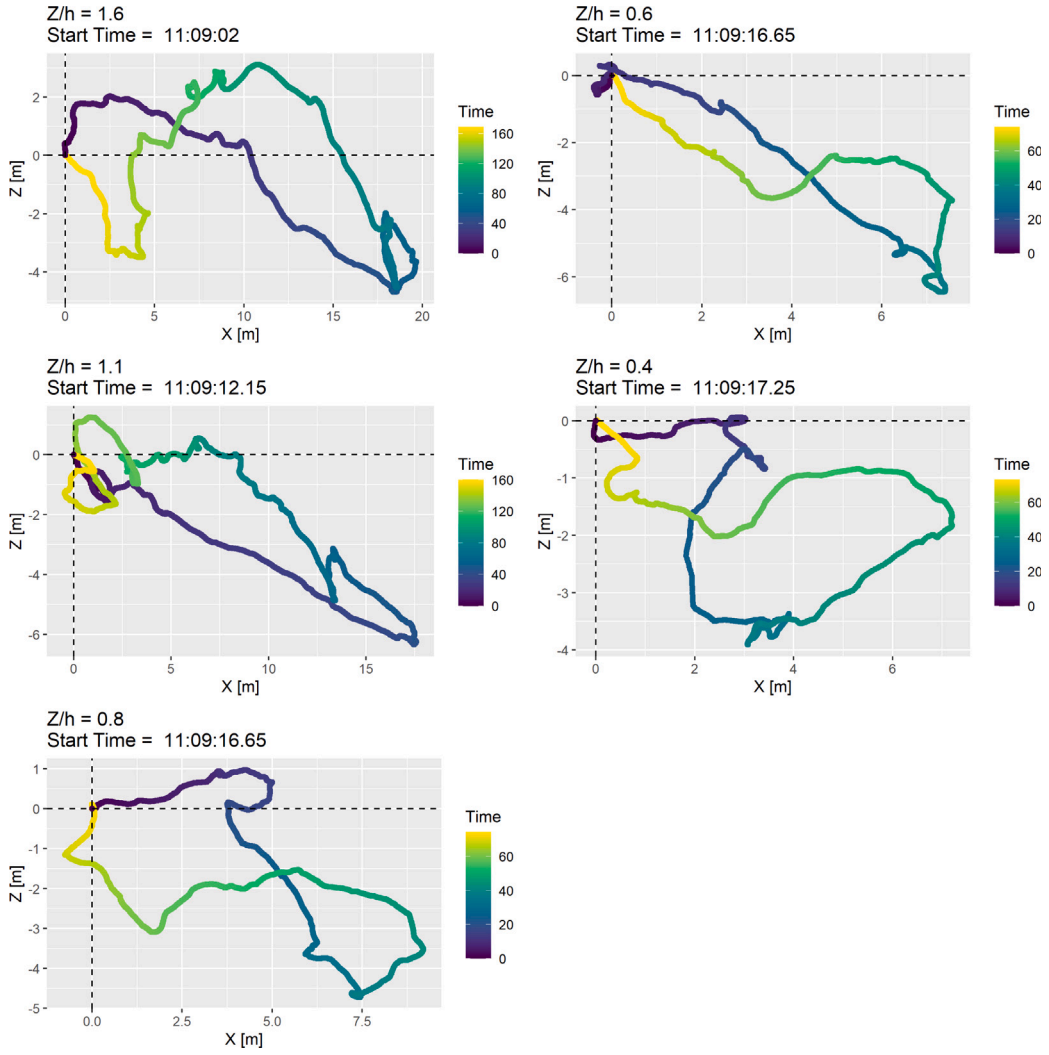

Fig. 3. Two-dimensional IQA plots for 16 November 2019 at 11:00 LT (UTC-8) at VACE. The colors indicate time in seconds since the start of the coherent structure. Note the changes in scale, particularly in the horizontal, and in time, for the respective axes.

change in X. This indicates that although w' is negative, u' is near 0. After the sweep at $Z/h = 0.4$, there is a quiescent period with counter-gradient flux with a duration of 15 s before an ejection returns the eddy trajectory to the origin.

We integrated v' with respect to time in the same way we integrated u' and w' to determine the three-dimensional eddy trajectory. Fig. 4 shows the integrated octant analysis for the same structure. The trajectory is colored by temperature perturbations to depict a visualization of how the eddy trajectory changes its temperature during the coherent structure event. While Z_i represents the vertical displacement of the eddy path, Y_i shows the cross-stream change in eddy trajectory. Like Z_i, Y_i represents a change in direction. Y_i shows the turning of the wind, and it is likely to depend on the part of the hairpin vortex that passes the sensor. This cross-stream trajectory component (Y_i) could elucidate the portion of a hairpin vortex passing the sensor or directional shear momentum transfer caused by the eddy trajectory. Although the cross-stream component is not always examined in surface layer flows, our results show X_i and Y_i have similar magnitudes at all heights for this coherent structure.

At $Z/h = 1.6$, 1.1, and 0.8, the structure begins in a weak ejection before moving into a strong bulk sweep. The eddy moves into positive values of X_i as seen in Fig. 3. At all heights, there is also a strong Y_i component to the eddy; however, unlike X_i, Y_i is both positive and negative during this event. At heights $Z/h = 1.1$, 0.8, 0.6, and 0.4, the microfront occurs approximately 20 s after the identified start of the coherent structure. The temperature drop is collocated with the start of the sweep (where Z_i begins to decrease), consistent with the method of using the drop in a temperature ramp to identify microfronts as in Gao et al. (1989). This supports the method of using the temperature signal to identify microfronts.

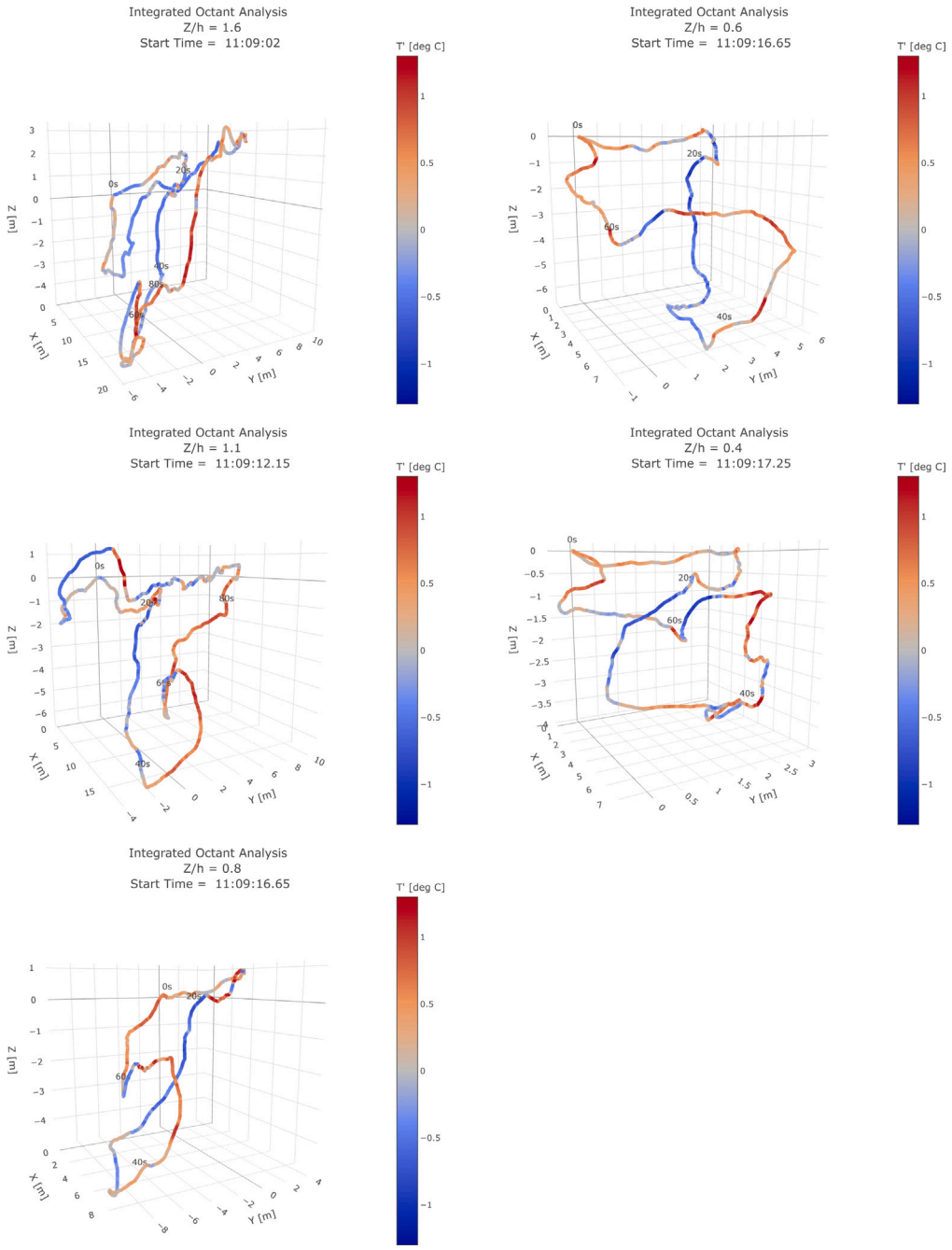

Fig. 4. Three-dimensional IQA plots for 16 November 2019 at 11:00 LT (UTC-8) for the VACE study. The colors indicate temperature perturbation. Times since the start of the structure are printed on the graph to indicate the direction of the structure. The supplemental material for this study includes an interactive version of this figure.

Much of the earlier framework for detecting and evaluating coherent structures uses only the u' and w' components of the velocity field, treating the cross-stream velocity as negligible. Our results imply that cross-stream velocity is an important component in coherent structures, and the cross-stream velocity perturbations can be as strong as the streamwise velocity perturbations (Fig. 4). For example, during the sweep at $Z/h = 0.4$, the two-dimensional plot (Fig. 3) shows that the eddy moves down in the Z_i direction but does not change in the X_i direction. In the three-dimensional plot, it is apparent that there is a strong cross-stream velocity movement.

In the two-dimensional case (Fig. 3), there is no discernible ejection at Z/h = 1.1, but we see a weak ejection corresponding to a temperature ramp in the 3D case approximately 10 s after the start of the coherent structure was identified. In the 10 s between the start of the ejection and start of the sweep, the Z position changes from −1.47 m to −0.67 m, the X position stays relatively constant (1.85 m to 1.39 m), but the Y position changes from 1.56 m to 5.05 m. This indicates that, in this case, the ejection is sustained almost entirely by the cross-stream contribution at $Z/h = 1.1$.

The direction of Y_i changes at approximately the same time at all levels. By considering the theoretical structure of the double-headed hairpin vortex (Finnigan et al., 2009), the change in the Y_i direction could represent the transition between two legs within a hairpin vortex or the transition from the head-up ejection vortex to the head-down sweep vortex. The Y_i direction component is also consistent with continuity concepts and the maintenance of coherent structures over a period of time. The turning in the Y_i direction is evident at all heights, but the magnitude of Y_i increases with height, like the

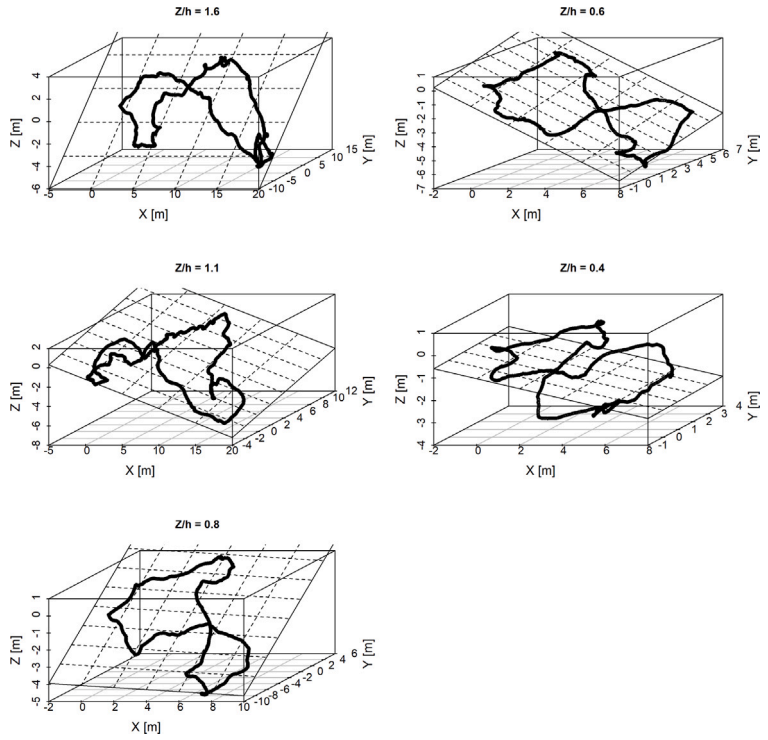

Fig. 5. Planar fits for the three-dimensional IQA plots for 16 November 2019 at 11:00 LT (UTC-8) for the VACE study. The black line is the eddy trajectory, and the plane represents the fitted trajectory for Z_i as a function of X_i and Y_i.

Table 2
Planar fit equations for 19 November 2019 for the coherent structure at 11:09 LT (UTC-8) for the VACE study.

Height (Z/h)	Plane	RMSD	r^2
0.4	$Z = -0.22X + 0.03Y - 1.00$	1.18	0.10
0.6	$Z = -0.67X + 0.26Y - 0.85$	0.71	0.87
0.8	$Z = -0.06X + 0.39Y - 0.18$	0.32	0.96
1.1	$Z = -0.30X + 0.23Y - 0.31$	0.66	0.88
1.6	$Z = +0.00X + 0.47Y - 1.47$	0.74	0.90

strength of the coherent structures. For interested readers, we refer to the supplemental material for an interactive version of Fig. 4.

Eddy trajectories can be fit with unique planes as evident in Fig. 4. Each plane can be approximated as the preferred 3-D direction for the coherent structure. Table 2 includes the equation for the plane, the coefficient of determination (r^2), and root mean square deviation (RMSD) for the fit for this event at each level. Fig. 5 shows the three-dimensional eddy trajectory and the planar fit of the eddy trajectory. At all levels, as Z_i increases, X_i decreases. This is consistent with an along-gradient momentum flux. At all heights, Z_i has a strong dependence on Y_i. The impact of Y_i is lowest close to the surface and greatest near the top of the canopy and at $Z/h = 1.6$. The plane at $Z/h = 0.4$ has the poorest fit to the data. The best fit occurs at $Z/h = 0.8$ where studies have shown the strength of the temperature ramps are strongest (Gao et al., 1992). This is also the region with the highest wind shear, so the planes fitting well could be related to the wind-shear dominated turbulence in this region.

In Fig. 5, the planes are dictated by the X_i and Y_i coefficients. Near the surface, there is little tilt in the Y-direction, but at the top of the canopy, the Y_i component is stronger than the X_i component. We have identified two hypotheses to explain this phenomenon. The first hypothesis is that the plane depends on the component of the hairpin vortex that passes the sensor arrays. At the highest levels, when the structure passes the sensor, the crosswind component is stronger than the streamwise component. This could occur if the sensors were measuring at the top or bottom faces of a hairpin vortex. The second hypothesis is associated with the maintenance of the microfront slope over the lifetime of coherent structures. Because the longitudinal wind is stronger above the canopy than within the canopy, to maintain a relatively constant microfront slope over time, and considering continuity, a stronger cross-stream component would be needed above the canopy than within the canopy. Otherwise, the microfront would quickly deform by steepening its slope from the higher longitudinal velocity above the canopy rather than below. Near the surface, all three components are weaker, and the plane is closer to the horizontal.

Following Gao et al. (1989), Fig. 6 is a time–height plot with temperature contours and wind vectors. The top panel has the $u'w'$ vectors and the bottom plot has the $v'w'$ vectors. The temperature contours indicate the microfront is tilted forward in time away from the surface. The $u'w'$ vectors show that ahead of the microfront, there is a weak ejection. A strong sweep occurs starting at the microfront and continues for 10 s after the microfront.

Like Gao et al. (1989), negative times occur before the microfront and positive times occur after it, allowing Fig. 6 to be interpreted as a cross-section with the longitudinal distance increasing from left to right, in the quasi-Lagrangian interpretation of the moving coherent structure. The $u'w'$ vectors show the same patterns as Gao et al. (1989). Just before the microfront, there is an ejection. After the microfront, there is a sweep that persists for about 15 s. The strongest vectors in $u'w'$ occur at $Z/h = 1.1$. During the sweep (time = +8 s), at $Z/h = 0.4$, there seems to be a counter-gradient momentum flux. At the same time, the other levels are showing an ejection, so there may be a momentum sink between $Z/h = 0.4$ and $Z/h = 0.6$.

The middle panel of Fig. 6 displays the $v'w'$ vectors. Before the front, the $v'w'$ vectors are weak and w' dominates. The $v'w'$ vectors are strongest above the canopy and weak near the surface. As the microfront approaches, the magnitude of v' increases, and v' peaks just after the passage of the microfront. Its sign changes from positive or near zero ahead of the front to strongly negative after the microfront. Above the canopy, $v'w'$ is approximately the same magnitude as $u'w'$. This could be associated with how the hairpin vortices and associated

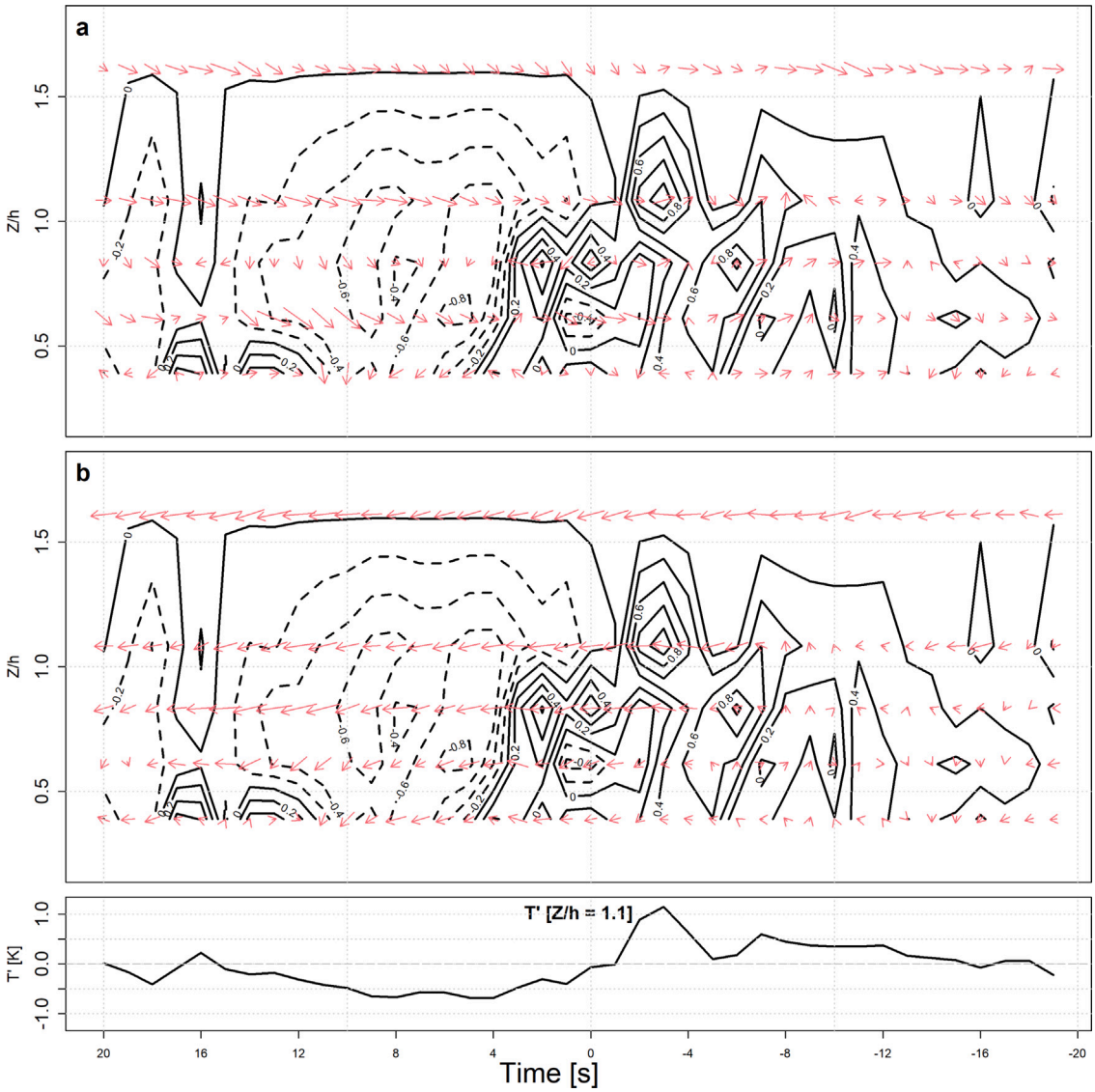

Fig. 6. The $\sqrt{u'^2 + w'^2}$ and $\sqrt{v'^2 + w'^2}$ vectors with temperature contours for 16 November 2019 at 11:00 LT (UTC-8) for the VACE study. Negative time is time before the microfront, zero time is the microfront, and positive time is the time after the microfront. The top and middle panels have the temperature contours. (a) The top plot has the $\sqrt{u'^2 + w'^2}$ vectors and (b) the middle plot has the $\sqrt{v'^2 + w'^2}$ vectors. (c) The bottom panel is the temperature signal at $Z/h = 1.1$.

flow patterns are sampled by the sensor array or the maintenance of the microfrontal structure, as discussed earlier.

3.1.2. Canopy Horizontal Array Turbulence Study

For the CHATS experiment, we selected one coherent structure that corresponds to a microfront with a temperature ramp amplitude of 1°C. The coherent structure began at 15:13 LT (UTC-8) on June 6, 2007. The event is identified earliest at $Z/h = 1.0$. It is identified within 5 s at all heights between $Z/h = 0.45$ and 1.4. This event was not identified as a structure at the two lowest ($Z/h = 0.15$, 0.3) and highest ($Z/h = 2.3$, 2.9) measurement heights. We hypothesize that the coherent structure was not identified at the bottom heights because the turbulence was damped by the bottom of the canopy. It was not identified far above the canopy because the detection method targets shear-driven turbulence, which is highest near the top of the canopy. The shear-driven eddies near the canopy top originate from 2–3 times the canopy height (Gao et al., 1989; Paw U et al., 1992; Su and Paw U, 2023; Zhang et al., 1992). Fig. 7 shows the two-dimensional IQA for select heights.

Above the canopy, the event begins in a sweep where u' is near zero. Inside of the canopy, there is a weak ejection before the bulk sweep begins 10 s after the start of the event. At all levels, the bulk sweep lasts 20 s. The eddy travels over 20 m in the X_i direction at $Z/h =$ 1.8, 1.1, and 0.9. The eddy travels between 10 and 20 m in the Z_i direction at all levels. The event is strongest at the top of the canopy ($Z/h = 1.1$) as expected, and the total distance in X_i and Z_i is 56 m as calculated from Eq. (4). The strength decreases as Z/h decreases inside of the canopy. The strength also decreases as Z/h increases above the canopy, though not as much as within the canopy, which is consistent with the idea that maximum shear occurs near the canopy top, driving the coherent structure dynamics. Above the canopy, the ejection begins immediately after the sweep, and it returns the eddy position to the origin. Inside of the canopy, there are short periods of counter-gradient flow where either u' or w' are near zero before the next ejection begins. These periods arise from the intermittency of the turbulence, so there is a separation between the end of one ejection and the start of the subsequent sweep.

Fig. 8 shows the three-dimensional plot of the same coherent structure for the same levels. Like Fig. 4, the line is colored by the temperature perturbations. At $Z/h = 0.45$ and $Z/h = 0.75$, the temperature drop corresponds with the start of the bulk sweep period. The temperature is cold through the sweep and warms during the ejection, with the maximum temperature occurring just before the end of the event. This

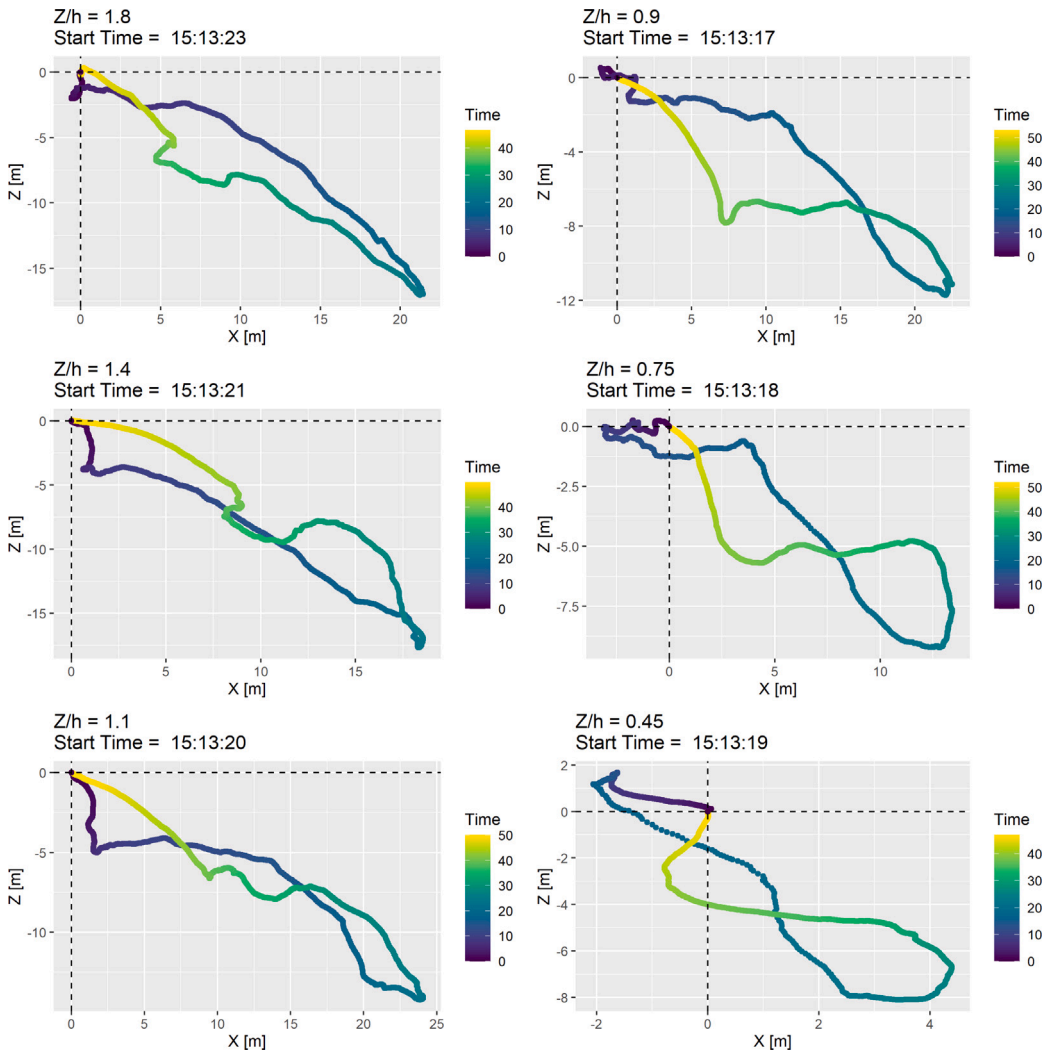

Fig. 7. Two-dimensional IQA plots for 06 June 2007 at 15:00 LT at the CHATS experiment. The colors indicate time in seconds since the start of the coherent structure.

is consistent with the surface renewal paradigm that under unstable stratification, cold air from above the canopy is drawn downward in the sweep and then warmed by the canopy elements and the soil surface before being ejected (Paw U and Su, 1994; Paw U et al., 1995).

Like in VACE, the Y_i component shows the turning of the wind during the coherent structure. At all levels, the Y_i component turns at the end of the sweep and again at the start of the next ejection. The magnitude of the Y_i component is largest above the canopy at Z/h = 1.8 and Z/h = 1.4. At all heights, the shape of the eddy looks similar, although there is less turning near the bottom of the canopy. Like with Fig. 4, we encourage interested readers to refer to the supplemental material for an interactive version of Fig. 8.

Each eddy trajectory can be fit with a plane (Fig. 9). At all heights, as Z_i decreases, X_i increases, which indicates these eddies are responsible for along-gradient momentum flux. At all heights, there is a negative Y_i tilt to the plane. This could suggest that the same portion of the turbulent coherent structure, or hairpin vortex, passes the sensors at all heights. Near the top of the canopy (Z/h = 0.75 and 0.9), the Y_i coefficient is almost as large as the X_i coefficient.

Table 3 has the equations and fits for the planes at all levels. Like in VACE, eddies do not fit the plane well at the bottom of the canopy (Z/h = 0.15). In this case, the coherent structure did not reach the bottom of the canopy. The planes fit best near the top of the canopy between Z/h = 0.45 and Z/h = 2.3. At the top of the canopy and near the surface, the Y_i coefficient is greater than or equal to the X_i coefficient. This supports the idea that the wind must turn as it approaches the no-slip surface condition to conserve mass and momentum. The Y_i component is small just above the canopy.

Table 3
Planar fit equations for 06 June 2007 at 15:13 LT at the CHATS experiment.

Height (Z/h)	Plane	RMSD	r^2
0.15	$Z = +0.16X + 0.21Y - 2.42$	3.29	0.31
0.30	$Z = -0.05X - 0.41Y - 1.46$	2.94	0.61
0.45	$Z = -1.33X - 0.24Y - 1.44$	1.31	0.82
0.60	$Z = -0.70X - 0.26Y - 1.34$	1.21	0.77
0.75	$Z = -0.58X - 0.47Y - 0.77$	1.12	0.85
0.90	$Z = -0.42X - 0.42Y - 0.30$	1.30	0.88
1.00	$Z = -0.45X - 0.08Y - 0.67$	1.15	0.91
1.10	$Z = -0.46X - 0.02Y - 1.38$	1.41	0.86
1.25	$Z = -0.54X - 0.04Y - 1.00$	1.42	0.89
1.40	$Z = -0.76X - 0.11Y - 0.32$	1.78	0.87
1.80	$Z = -0.68X - 0.10Y - 0.27$	2.57	0.90
2.30	$Z = -0.26X - 0.19Y - 4.23$	2.12	0.82
2.90	$Z = -0.14X - 0.20Y - 5.87$	2.90	0.72

The time–height plot as shown in Gao et al. (1989) for this event supports the results for IQA (Fig. 10). The temperature contours show that the microfront is tilted so that it lags in time at the surface, representing a spatial slope to the microfront and the time it takes the vertically descending sweep motion to traverse into the canopy

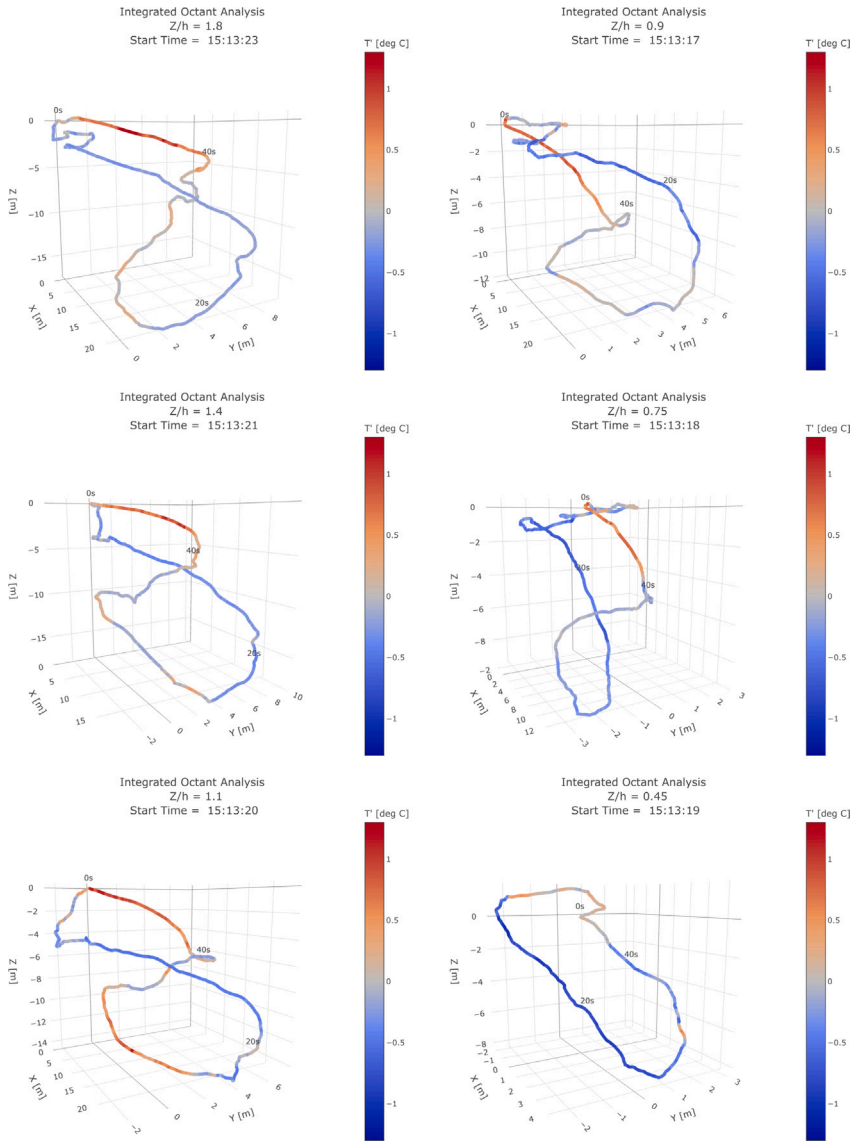

Fig. 8. Three-dimensional IQA plots for 06 June 2007 at 15:00 LT at the CHATS experiment. The colors indicate temperature perturbation. Times since the start of the structure are printed on the graph to indicate the direction of the structure. Please refer to the supplemental material for an interactive version of this figure.

air space (Gao et al. 1989). It also shows that the temperature front does not reach the surface; furthermore, it does not pass $Z/h = 0.5$. This indicates that the coherent structures dampen near the ground because of the no-flow boundary conditions. The $u'w'$ shows the strong sweep that occurs just after the microfront. The turbulent momentum stress magnitudes are strongest between $Z/h = 1.4$ and $Z/h = 0.6$. The strongest sweep starts about 10 s after the passage of the microfront. The sweep occurring this long after the microfront might indicate that the coherent structure that occurred downwind was fossilized when it reached the sensors. At the passage of the microfront, the velocity field is dominated by the w' term, which was also observed in the IQA plots. Until the strong sweep 10 s after the microfront, the velocity field in and below $Z/h = 0.5$ shows little response to the event. Before the microfront, there is a strong ejection between $Z/h = 0.6$ and $Z/h = 1.8$ that lasts 10 to 15 s. Because the IQA was triggered 10 s before the microfront at most levels, the strong ejection might have been paired to the previous coherent structure. Above $Z/h = 2$, there is a weak $u'w'$ response to the microfront. There is an ejection that occurs near time = 0 s. Otherwise, the vectors are dominated by the u' component, which shows that the sign of u' changes at the microfront.

The velocity field in $v'w'$ shows similar results to that of the $u'w'$ velocity field: the components in v' are largest 10 to 20 s after the passage of the microfront. Before the microfront, the w' signal dominates. The sign of v' changes near the microfront. The $v'w'$ vectors show a weak circular motion from time = -8 s to time = +8 s from heights $Z/h = 0.45$ to $Z/h = 1.4$, where the temperature gradient is the strongest. This implies that the microfront is accompanied by the wind turning, which would be compatible with reports of mean directional wind shear sometimes occurring in plant canopies (Pyles et al., 2004) that would require a $v'w'$ component loosely analogous to turbulent Ekman dynamics. This phenomenon is also evident in Fig. 8 when the Y_i direction changes near the sweep.

3.2. IQA statistics

In addition to IQA being useful for looking at individual coherent structures, it can also be applied to longer periods of time to determine the mean characteristics of the coherent structures. The total distance of each structure (Eq. (4)) is similar to a measure of the size or strength of individual coherent structures, and it provides a form of an integral length scale for coherent structures. Because there is not yet a method to signal the end of these events, the distance for each structure includes the quiescent period before the next coherent

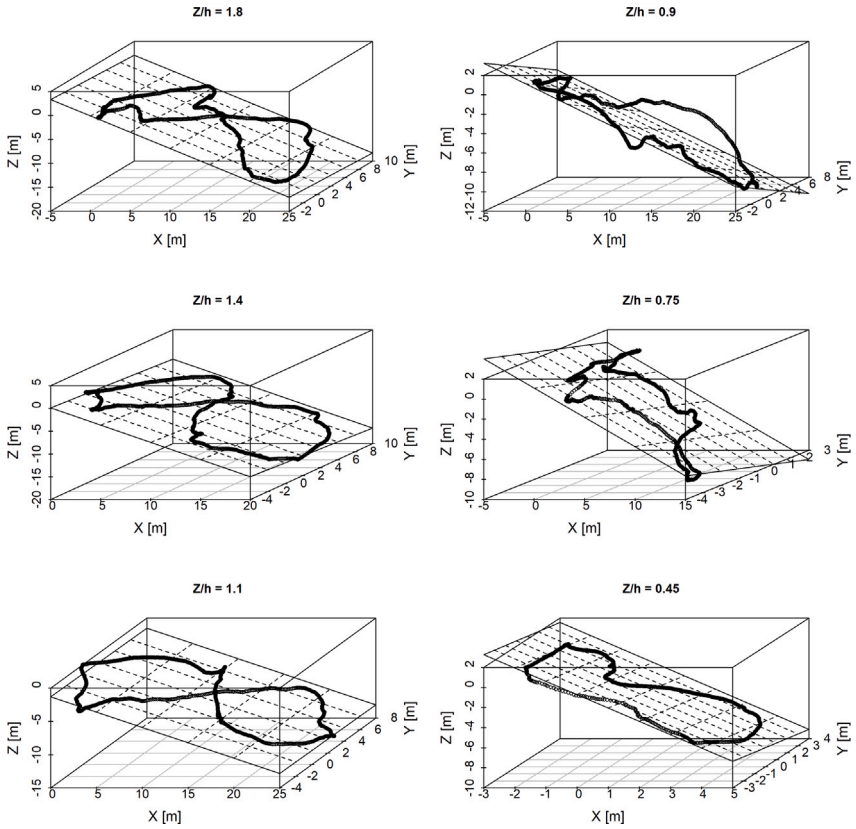

Fig. 9. Planar fits for the three-dimensional IQA plots for 06 June 2007 at 15:00 LT at the CHATS experiment. The black line is the eddy trajectory, and the plane represents the fitted trajectory for Z_i as a function of X_i and Y.

structure. Future work will investigate methods for determining the end times of the structures. At night, when the turbulence is intermittent, our coherent structure identification method identifies fewer structures. Because $uTKE$ is lower during the night than during the day, averaging these nighttime events can provide reasonable results for the average strength.

The median distance scale for the coherent structures for the entire VACE campaign separated by season and hour of the day in VACE is shown in Fig. 11. At $Z/h = 0.4$ and $Z/h = 0.6$, the median magnitudes for X_i and Y_i are nearly the same. Above the canopy, the X_i component is larger than the Y_i component. Although Z_i is less than X_i and Y_i at all levels, Z_i constitutes a larger component of the total distance closer to the surface than above the canopy. During all seasons, the coherent structures are longer during the day than at night. The peak distance occurs from early to midafternoon. At night, the spikes in the distance signals could be the result of intermittent turbulence, or they could indicate the presence of sub-mesoscale motions (Mahrt, 2010).

For all seasons in VACE, the distance of the structures decreases close to the surface, and the longest structures occur at $Z/h = 1.6$. In the leaf and leaf-out periods, the magnitudes of coherent structures clearly show a diurnal pattern; however, during the leafless period, this pattern is not as clear. The distance of structures in the winter are shorter than the periods with leaves. The leaf-out period has the longest structures at all levels. This effect is likely due to both a shear effect (foliated trees generate more shear-driven turbulence) and a seasonal effect (increased surface heating in the spring and summertime produces more buoyancy-generated turbulence than the wintertime). The size of each component of the coherent structures ranges from 60 m above the canopy to 15 m near the surface.

CHATS results exhibit the same diurnal pattern as VACE, but they better show the strength of each coherent structure with height. Fig. 12 includes the profiles of the X, Y_i, and Z_i distances split between the leafless and the leaf periods. During the leafless period, the structures with maximum strength occur near the top of the canopy ($Z/h = 0.9$). The coherent structure sizes increase with height inside of the canopy. Above the canopy, the distance is constant with height, which was also seen over a low roughness surface in Mangan et al. (2022). Below $Z/h = 0.6$, the magnitudes of X_i and Y_i are the same, but Y_i decreases with respect to X_i above that point. Z_i is about half the size of X_i near the canopy top.

During the leaf period, the distances of the coherent structures peak at $Z/h = 0.6$, near the sub-canopy maximum. This subcanopy maximum is typically located just below the maximum leaf area index in the crown because of its low wind shear (Pyles et al., 2004; Shaw et al., 1974). As seen in the no-leaf period, X_i and Y_i are the same magnitude below $Z/h = 0.75$. The magnitude of Z_i is about 90% that of X_i and Y_i in the middle of the canopy. X_i peaks at the top of the canopy before decreasing slightly with height. Y_i and Z_i barely change with height above the canopy.

In addition to the median distances from IQA that provide information about the characteristic strength of coherent structures, the planar fit of the eddy trajectories can indicate if there are preferred eddy trajectories, potentially related to turbulent flow patterns associated with the coherent structures. Although we hypothesize that the planar tilt of the eddies potentially relates to the portion of a hairpin vortex or other flow structures that pass the sensor, a wind direction dependence for the planes could suggest that there is a characteristic vortex associated with roughness elements or geometries related to the sensor location. For example, in an orchard, a wind direction dependence on the plane could indicate channel flow up the row or a vortex shed from a nearby individual tree. With the CHATS data, one might expect to see channel flow, whereas, with the VACE data, one might expect to see channel flow or a vortex from an individual tree because the observations for CHATS are taken in the interrow space, and the observations for VACE are taken from within a crown.

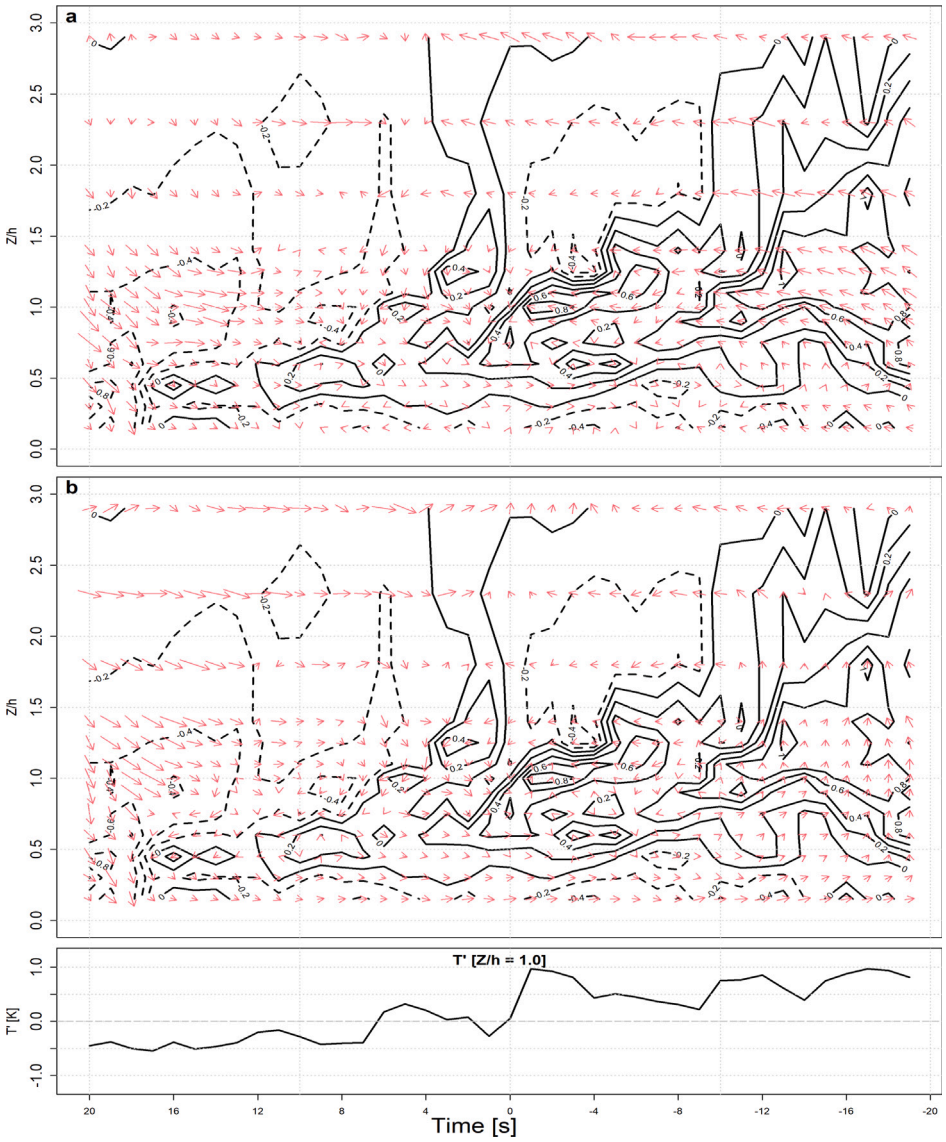

Fig. 10. The $\sqrt{u'^2 + w'^2}$ and $\sqrt{v'^2 + w'^2}$ vectors with temperature contours for 06 June 2007 at 15:00 LT at the CHATS experiment. Negative time is time before the microfront, zero time is the microfront, and positive time is the time after the microfront. The top and middle panels have the temperature contours. (a) The top plot has the $\sqrt{u'^2 + w'^2}$ vectors and (b) the middle plot has the $\sqrt{v'^2 + w'^2}$ vectors. (c) The bottom panel is the temperature signal at $Z/h = 1.0$.

The slope of the regression plane with Z_i as a function of X_i and Y_i has the general form

$$Z = aX + bY + c \tag{5}$$

where a and b describe the slope of the plane in the X_i and Y_i axis, respectively and c is the offset of the plane on the Z_i axis. Hereafter, X_i and Y_i coefficients refer to a and b, respectively.

From Fig. 13, there is no apparent average dependence of the planar fits with wind direction, as shown by the X_i and Y_i coefficients split by wind direction (left columns) and wind speeds (right columns) for each height for all periods of VACE. There are high X_i and Y_i coefficients occurring for many different wind directions, but over time, the planes average to zero. In particular, winds from the southeast had coefficients with higher magnitude than other wind directions at $Z/h = 0.8$ and $Z/h = 0.4$, but when averaged over wind direction, the plane was horizontal.

The two right-most columns on Fig. 13 show the X_i and Y_i coefficients for the planar fit versus the wind speed at each height for VACE. At low wind speeds, there is more likely to be a tilt in the planar fit for eddy trajectories. At all wind speeds, including low wind speeds, the average plane is horizontal.

The results from CHATS are like those of VACE: there is no wind direction dependence on the eddy planes, but there is a wind speed dependence. Although there are planes that fit the eddy trajectory for any given coherent structure, there does not appear to be a typical plane for either study. The tilt of the planes are more likely to occur at low wind speeds. When the wind speeds are higher, the streamwise velocity is likely to be much greater than the vertical and cross-stream velocities, so the planes become more parallel to the surface.

4. Conclusions

Three-dimensional IQA was calculated with case studies for two orchard experiments: CHATS and VACE. The IQA method allows us both to trace the trajectories of turbulent coherent structures and to link the momentum components of turbulence to the temperature component. The temperature drops occur at the same time as the sweep starts, consistent with previous studies. The three-dimensionality of the structures shows that the cross-stream Y_i component is approximately the same strength as the X_i component, demonstrating a turning of the flow in the structure during sweeps. The cross-stream velocity is a

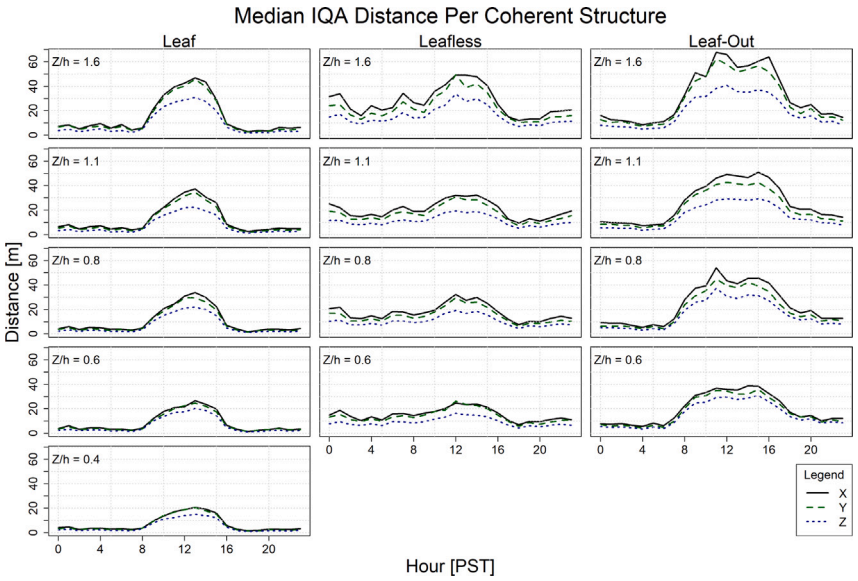

Fig. 11. The median distances for each wind direction split by hour of the day for each measurement period in VACE.

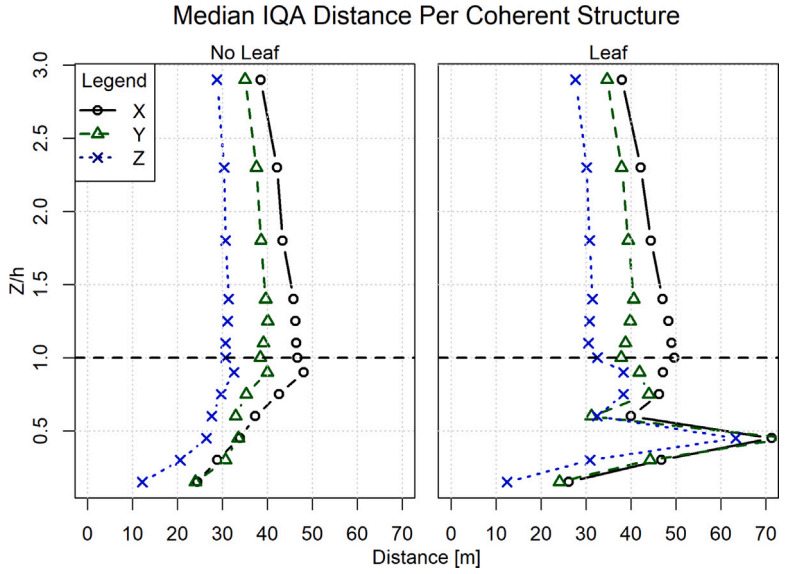

Fig. 12. The median component distance for all coherent structures by height for each period of CHATS.

non-trivial component in the complex three-dimensionality of turbulent coherent structures.

Moreover, IQA for individual coherent structures shows that there are preferred planes for eddy trajectories. The plane changes with every coherent structure when the observations are at a fixed Eulerian location. Although the planes of all coherent structures do not average to a horizontal plane for every half hour period, over several weeks, they do average to a horizontal plane. The planes do not seem to be a function of wind direction, suggesting that the orchard row structures in both the CHATS and VACE experiments did not substantially affect the turbulent coherent structures, and the proximity of an individual tree crown to sonic anemometers did not strongly influence the ability of the sensors to characterize the structures. The scale of the crown effects are smaller than that of these observed coherent structures. The individual planar tilts were higher at low wind speeds, while the tilts became more horizontal at higher wind speeds, as might be expected. Our planar tilt analysis is compatible with sampling different portions of hairpin vortices passing by the sensor arrays, although other turbulent coherent structure flow patterns might also explain the individual planar tilt variation.

We find that there are no appreciable differences in the characteristics of coherent structures observed in the interrow of orchards compared with those observed adjacent to the tree canopy for our selected events. By combining data from CHATS and VACE, we can conclude that the orchard structure does not create unique vortices dependent on the wind direction in sparse orchards as long as the vortices are persistent on the scale of the coherent structures. Seasonally, the strongest turbulence occurs when the trees are foliated, compared to leafless conditions. This suggests that drag-induced shear is an important aspect in the creation of strong coherent structures over vegetation. Because periods of stronger buoyancy fluxes can be collocated with periods of high wind shear inside of a crown, buoyancy-driven turbulence may also play a role the maintenance of turbulent coherent structures. Future work should be done to separate the effects of shear-driven turbulence from buoyancy-driven turbulence.

Because this research includes case studies for turbulence specifically in orchards, further work needs to be done to expand the research

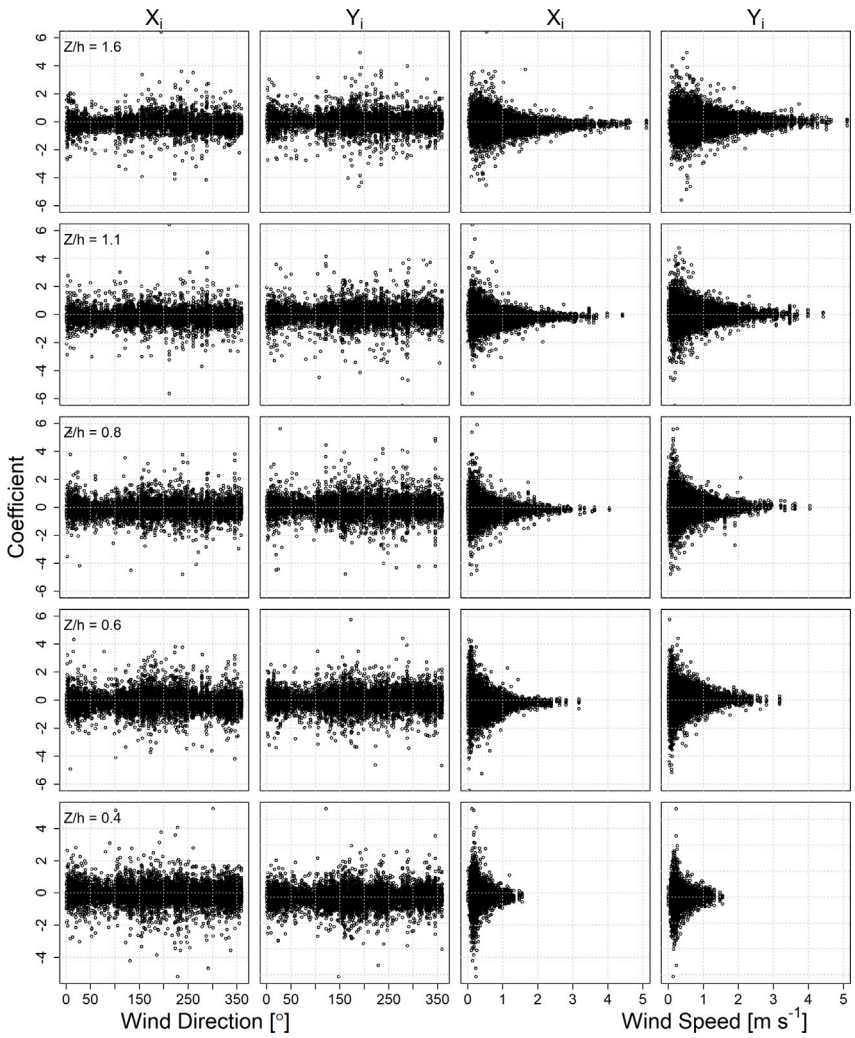

Fig. 13. The VACE coefficients for planar fit. The two columns on the left are the X_i and Y_i coefficients for wind direction. The two columns on the right are the X_i and Y_i coefficients by wind speed. All plots are for all time periods of VACE.

in other vegetation types to make these results generalizable. However, by calculating statistical measures based on IQA, we are able to evaluate the relative size of coherent structures so that we can compare with other land surfaces. IQA allows us to visualize the 3D trajectory of turbulent coherent structures based on a single-point measurement. Although the method does not allow for the quantification of fluxes from individual structures, by visualizing their path with respect to scalars provides a tool to expand our understanding of the mechanics of turbulence. IQA is a promising tool for quantifying the nature of turbulent coherent structures in the atmospheric surface layer.

CRediT authorship contribution statement

Mary Rose Mangan: Conceptualization, Formal analysis, Validation, Visualization, Writing – original draft. **Holly J. Oldroyd:** Conceptualization, Supervision, Writing – review & editing, Methodology. **Kyaw Tha Paw U:** Conceptualization, Methodology, Supervision, Writing – review & editing. **Jenae M. Clay:** Data curation, Writing – review & editing. **Kosana Suvočarev:** Data curation, Supervision, Writing – review & editing.

Declaration of competing interest

The authors declare that they have no known competing financial interests or personal relationships that could have appeared to influence the work reported in this paper.

Data availability

Data will be made available on request.

Acknowledgments

Funding for VACE came in part from the California Cherry Board Grant No. 20-CCB5400-11. Partial support came from the United States Department of Agriculture National Institute of Food and Agriculture, Hatch Project CA-D-LAW-4526H. This work was partially funded by NSF Physical and Dynamic Meteorology (PDM) Grant No. 1848019. We would like to acknowledge Renata Minhoni, Emma Ware, and Shicheng Yan, who assisted with the VACE field campaign. We would like to acknowledge Jonathan Huynh and David Edgar for their work supporting the initial exploration of the IQA method. We would like to thank the two anonymous reviewers for their detailed comments which greatly improved this study.

Appendix A. Supplementary data

Supplementary material related to this article can be found online at https://doi.org/10.1016/j.agrformet.2024.110042.

References

Adrian, R.J., 2007. Hairpin vortex organization in wall turbulence. Phys. Fluids 19 (4), 041301. http://dx.doi.org/10.1063/1.2717527, URL: https://aip.scitation.org/doi/10.1063/1.2717527. Publisher: American Institute of Physics.

Antonia, R.A., Atta, C.W.V., 1978. Structure functions of temperature fluctuations in turbulent shear flows. J. Fluid Mech. 84 (3), 561–580. http://dx.doi.org/10.1017/S0022112078000336, URL: https://www.cambridge.org/core/journals/journal-of-fluid-mechanics/article/structure-functions-of-temperature-fluctuations-in-turbulent-shear-flows/57E08DB10E3875F2012E7D60B713A994. Publisher: Cambridge University Press.

Baldocchi, D.D., Meyers, T.P., 1988. Turbulence structure in a deciduous forest. Bound.-Layer Meteorol. 43 (4), 345–364. http://dx.doi.org/10.1007/BF00121712.

Bernard, P.S., 2011. The hairpin vortex illusion. J. Phys. Conf. Ser. 318 (6), 062004. http://dx.doi.org/10.1088/1742-6596/318/6/062004, Publisher: IOP Publishing.

Bisset, D.K., Antonia, R.A., Browne, L.W.B., 1990. Spatial organization of large structures in the turbulent far wake of a cylinder. J. Fluid Mech. 218, 439–461. http://dx.doi.org/10.1017/S0022112090001069, URL: https://www.cambridge.org/core/journals/journal-of-fluid-mechanics/article/spatial-organization-of-large-structures-in-the-turbulent-far-wake-of-a-cylinder/55222C9FBFA3FE6600E298944A3FA85E.

Blackwelder, R.F., Kaplan, R.E., 1976. On the wall structure of the turbulent boundary layer. J. Fluid Mech. 76 (1), 89–112. http://dx.doi.org/10.1017/S0022112076003145, URL: https://www.cambridge.org/core/product/identifier/S0022112076003145/type/journal_article.

Chen, C.-H.P., Blackwelder, R.F., 1978. Large-scale motion in a turbulent boundary layer: a study using temperature contamination. J. Fluid Mech. 89 (1), 1–31. http://dx.doi.org/10.1017/S0022112078002438, URL: https://www.cambridge.org/core/journals/journal-of-fluid-mechanics/article/largescale-motion-in-a-turbulent-boundary-layer-a-study-using-temperature-contamination/DDBC02D06DD6BFE9F8F579434CFFBA32.

Collineau, S., Brunet, Y., 1993. Detection of turbulent coherent motions in a forest canopy part II: Time-scales and conditional averages. Bound.-Layer Meteorol. 66 (1–2), 49–73. http://dx.doi.org/10.1007/BF00705459, URL: http://link.springer.com/10.1007/BF00705459.

Denmead, O.T., Bradley, E.F., 1987. On scalar transport in plant canopies. Irrig. Sci. 8 (2), 131–149. http://dx.doi.org/10.1007/BF00259477.

Dupont, S., Patton, E.G., 2012. Momentum and scalar transport within a vegetation canopy following atmospheric stability and seasonal canopy changes: the CHATS experiment. Atmos. Chem. Phys. 12 (13), 5913–5935. http://dx.doi.org/10.5194/acp-12-5913-2012, URL: https://www.atmos-chem-phys.net/12/5913/2012/. Publisher: Copernicus GmbH.

Farge, M., 1992. Wavelet transforms and their applications to turbulence. Annu. Rev. Fluid Mech. 24 (1), 395–458. http://dx.doi.org/10.1146/annurev.fl.24.010192.002143, URL: https://www.annualreviews.org/doi/10.1146/annurev.fl.24.010192.002143.

Finnigan, J.J., 1979. Turbulence in waving wheat. Bound.-Layer Meteorol. 16 (2), 181–211. http://dx.doi.org/10.1007/BF02350511, URL: https://link.springer.com/article/10.1007/BF02350511.

Finnigan, J.J., 2000. Turbulence in plant canopies. Annu. Rev. Fluid Mech. 32 (1), 519–571. http://dx.doi.org/10.1146/annurev.fluid.32.1.519.

Finnigan, J.J., Shaw, R.H., Patton, E.G., 2009. Turbulence structure above a vegetation canopy. J. Fluid Mech. 637, 387–424. http://dx.doi.org/10.1017/S0022112009990589, URL: https://www.cambridge.org/core/journals/journal-of-fluid-mechanics/article/turbulence-structure-above-a-vegetation-canopy/575D5DD5B6CFD8837D3C765E04216E41. Publisher: Cambridge University Press.

Fitzmaurice, L., Shaw, R.H., Paw U, K.T., Patton, E.G., 2004. Three-dimensional scalar microfront systems in a large-eddy simulation of vegetation canopy flow. Bound.-Layer Meteorol. 112 (1), 107–127. http://dx.doi.org/10.1023/B:BOUN.0000020159.98239.4a.

Gao, W., Shaw, R., Paw U, K.T., 1989. Observation of organized structure in turbulent flow within and above a forest canopy. Bound.-Layer Meteorol. 47, 349–377.

Gao, W., Shaw, R.H., U. Paw, K.T., 1992. Conditional analysis of temperature and humidity microfronts and ejection/sweep motions within and above a deciduous forest. Bound.-Layer Meteorol. 59 (1–2), 35–57. http://dx.doi.org/10.1007/BF00120685, URL: http://link.springer.com/10.1007/BF00120685.

Hari, P., Nikinmaa, E., Pohja, T., Siivola, E., Bäck, J., Vesala, T., Kulmala, M., 2013. Station for measuring ecosystem-atmosphere relations: SMEAR. In: Hari, P., Heliövaara, K., Kulmala, L. (Eds.), Physical and Physiological Forest Ecology. Springer Netherlands, Dordrecht, pp. 471–487. http://dx.doi.org/10.1007/978-94-007-5603-8_9.

Mahrt, L., 2010. Variability and maintenance of turbulence in the very stable boundary layer. Bound.-Layer Meteorol. 135 (1), http://dx.doi.org/10.1007/s10546-009-9463-6.

Mangan, M.R., Oldroyd, H.J., Paw U, K.T., Clay, J.M., Drake, S.A., Kelley, J., Suvočarev, K., 2022. Integrated quadrant analysis: A new method for analyzing turbulent coherent structures. Bound.-Layer Meteorol. http://dx.doi.org/10.1007/s10546-022-00694-w.

Misson, L., Baldocchi, D.D., Black, T.A., Blanken, P.D., Brunet, Y., Curiel Yuste, J., Dorsey, J.R., Falk, M., Granier, A., Irvine, M.R., Jarosz, N., Lamaud, E., Launiainen, S., Law, B.E., Longdoz, B., Loustau, D., McKay, M., Paw U, K.T., Vesala, T., Vickers, D., Wilson, K.B., Goldstein, A.H., 2007. Partitioning forest carbon fluxes with overstory and understory eddy-covariance measurements: A synthesis based on FLUXNET data. Agricult. Forest Meteorol. 144 (1), 14–31. http://dx.doi.org/10.1016/j.agrformet.2007.01.006.

Patton, E.G., Horst, T.W., Sullivan, P.P., Lenschow, D.H., Oncley, S.P., Brown, W.O.J., Burns, S.P., Guenther, A.B., Held, A., Karl, T., Mayor, S.D., Rizzo, L.V., Spuler, S.M., Sun, J., Turnipseed, A.A., Allwine, E.J., Edburg, S.L., Lamb, B.K., Avissar, R., Calhoun, R.J., Kleissl, J., Massman, W.J., Paw U, K.T., Weil, J.C., 2011. The canopy horizontal array turbulence study. Bull. Am. Meteorol. Soc. 92 (5), 593–611. http://dx.doi.org/10.1175/2010BAMS2614.1, URL: http://journals.ametsoc.org/doi/abs/10.1175/2010BAMS2614.1.

Paw U, K.T., Baldocchi, D.D., Meyers, T.P., Wilson, K.B., 2000. Correction of eddy-covariance measurements incorporating both advective effects and density fluxes. Bound.-Layer Meteorol. 97 (3), 487–511. http://dx.doi.org/10.1023/A:1002786702909, URL: http://link.springer.com/10.1023/A:1002786702909.

Paw U, K.T., Brunet, Y., Collineau, S., Shaw, R.H., Maitani, T., Qiu, J., Hipps, L., 1992. On coherent structures in turbulence above and within agricultural plant canopies. Agricult. Forest Meteorol. 61 (1–2), 55–68. http://dx.doi.org/10.1016/0168-1923(92)90025-Y, URL: https://linkinghub.elsevier.com/retrieve/pii/016819239290025Y.

Paw U, K.T., Qiu, J., Su, H.-B., Watanabe, T., Brunet, Y., 1995. Surface renewal analysis: a new method to obtain scalar fluxes. Agricult. Forest Meteorol. 74 (1–2), 119–137. http://dx.doi.org/10.1016/0168-1923(94)02182-J, URL: https://linkinghub.elsevier.com/retrieve/pii/016819239402182J.

Paw U, K.T., Su, H.-B., 1994. The usage of structure functions in studying turbulent coherent structures and estimating sensible heat flux. In: 21st Conf. on Agricultural and Forest Meteorology. San Diego, CA. Am. Meteorol. Soc, Boston, MA.

Priestley, C., 1959. Turbulent Transfer in the Lower Atmosphere. University of Chicago Press, Chicago.

Pyles, R.D., Paw U, K.T., Falk, M., 2004. Directional wind shear within an old-growth temperate rainforest: observations and model results. Agricult. Forest Meteorol. 125 (1), 19–31. http://dx.doi.org/10.1016/j.agrformet.2004.03.007, URL: https://www.sciencedirect.com/science/article/pii/S0168192304000851.

Raupach, M.R., 1981. Conditional statistics of Reynolds stress in rough-wall and smooth-wall turbulent boundary layers. J. Fluid Mech. 108, 363–382. http://dx.doi.org/10.1017/S0022112081002164, URL: https://www.cambridge.org/core/product/identifier/S0022112081002164/type/journal_article.

Raupach, M.R., Finnigan, J.J., Brunet, Y., 1996. Coherent eddies and turbulence in vegetation canopies: The mixing-layer analogy. Bound.-Layer Meteorol. 32.

Raupach, M.R., Shaw, R.H., 1982. Averaging procedures for flow within vegetation canopies. Bound.-Layer Meteorol. 22 (1), 79–90. http://dx.doi.org/10.1007/BF00128057, URL: http://link.springer.com/10.1007/BF00128057.

Shaw, R.H., Paw U, K.T., Gao, W., 1989. Detection of temperature ramps and flow structures at a deciduous forest site. Agricult. Forest Meteorol. 47 (2), 123–138. http://dx.doi.org/10.1016/0168-1923(89)90091-9, URL: http://www.sciencedirect.com/science/article/pii/0168192389900919.

Shaw, R.H., Silversides, R.H., Thurtell, G.W., 1974. Some observations of turbulence and turbulent transport within and above plant canopies. Bound.-Layer Meteorol. 5 (4), 429–449. http://dx.doi.org/10.1007/BF00123490.

Smith, F.B., Carson, D.J., Oliver, H.R., 1972. Mean wind-direction shear through a forest canopy. Bound.-Layer Meteorol. 3 (2), 178–190. http://dx.doi.org/10.1007/BF02033917.

Su, H., Paw U, K., 2023. Large-eddy simulation of Reynolds stress budgets in and above forests in neutral atmospheric boundary layers. Bound.-Layer Meteorol. 187, 457–500. http://dx.doi.org/10.1007/s10546-022-00758-x.

Theodorsen, T., 1952. Mechanism of turulence. In: Proceedings of Second Midwest Conference on Fluid Mechanics. Ohio State Univeristy, Columbus, OH.

Thomas, C., Foken, T., 2005. Detection of long-term coherent exchange over spruce forest using wavelet analysis. Theor. Appl. Climatol. 80 (2), 91–104. http://dx.doi.org/10.1007/s00704-004-0093-0.

Wallace, J.M., Eckelmann, H., Brodkey, R.S., 1972. The wall region in turbulent shear flow. J. Fluid Mech. 54 (1), 39–48. http://dx.doi.org/10.1017/S0022112072000515, URL: https://www.cambridge.org/core/journals/journal-of-fluid-mechanics/article/wall-region-in-turbulent-shear-flow/F38FABEC434430051BE92BAEDAE3EC14.

Watanabe, T., 2004. Large-eddy simulation of coherent turbulence structures associated with scalar ramps over plant canopies. Bound.-Layer Meteorol. 112 (2), 307–341. http://dx.doi.org/10.1023/B:BOUN.0000027912.84492.54, URL: http://link.springer.com/10.1023/B:BOUN.0000027912.84492.54.

Wilczak, J.M., 1984. Large-scale eddies in the unstably stratified atmospheric surface layer. part I: Velocity and temperature structure. J. Atmos. Sci. 41 (24), 3537–3550. http://dx.doi.org/10.1175/1520-0469(1984)041<3537:LSEITU>2.0.CO;2, URL: https://journals.ametsoc.org/doi/10.1175/1520-0469%281984%29041%3C3537%3ALSEITU%3E2.0.CO%3B2.

Wilczak, J.M., Oncley, S.P., Stage, S.A., 2001. Sonic anemometer tilt correction algorithms. Bound.-Layer Meteorol. 99 (1), 127–150. http://dx.doi.org/10.1023/A:1018966204465.

Wilson, N.R., Shaw, R.H., 1977. A higher order closure model for canopy flow. J. Appl. Meteorol. 16 (11), 1197–1205. http://dx.doi.org/10.1175/1520-0450(1977)016<1197:AHOCMF>2.0.CO;2, URL: https://journals.ametsoc.org/doi/abs/10.1175/1520-0450(1977)016%3C1197:AHOCMF%3E2.0.CO%3B2. Publisher: American Meteorological Society.

Wilson, J.D., Ward, D.P., Thurtell, G.W., Kidd, G.E., 1982. Statistics of atmospheric turbulence within and above a corn canopy. Bound.-Layer Meteorol. 24 (4), 495–519. http://dx.doi.org/10.1007/BF00120736.

Zaremba, L.L., Carroll, J.J., 1999. Summer wind flow regimes over the sacramento valley. J. Appl. Meteorol. Climatol. 38 (10), 1463–1473. http://dx.doi.org/10.1175/1520-0450(1999)038<1463:SWFROT>2.0.CO;2, Publisher: American Meteorological Society Section: Journal of Applied Meteorology and Climatology.

Zhang, C., Shaw, R., Paw U, K., 1992. Spatial characteristics of turbulent coherent structures within and above an orchard canopy. In: Schwartz, S., Slinn, W. (Eds.), Precipitation Scavenging and Atmosphere-Surface Exchange. Vol. 2, Hemisphere Publishing Co., Washington, pp. 741–751, chapter 10.